Figure S1

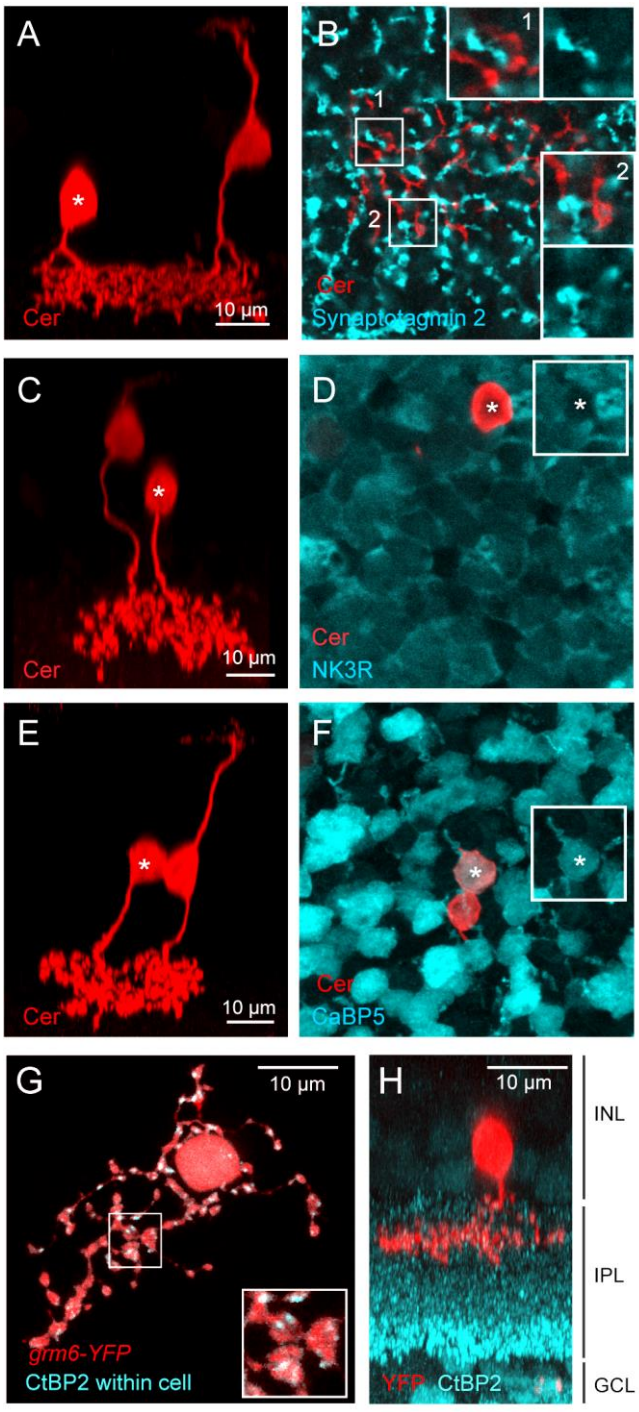
A
Cer
10 µm
B
1
2
Cer
Synaptotagmin 2
C
Cer
10 µm
D
Cer
NK3R
E
Cer
10 µm
F
Cer
CaBP5
G
10 µm
grm6-YFP
CtBP2 within cell
H
10 µm
YFP CtBP2
INL
IPL
GCL

Figure S2

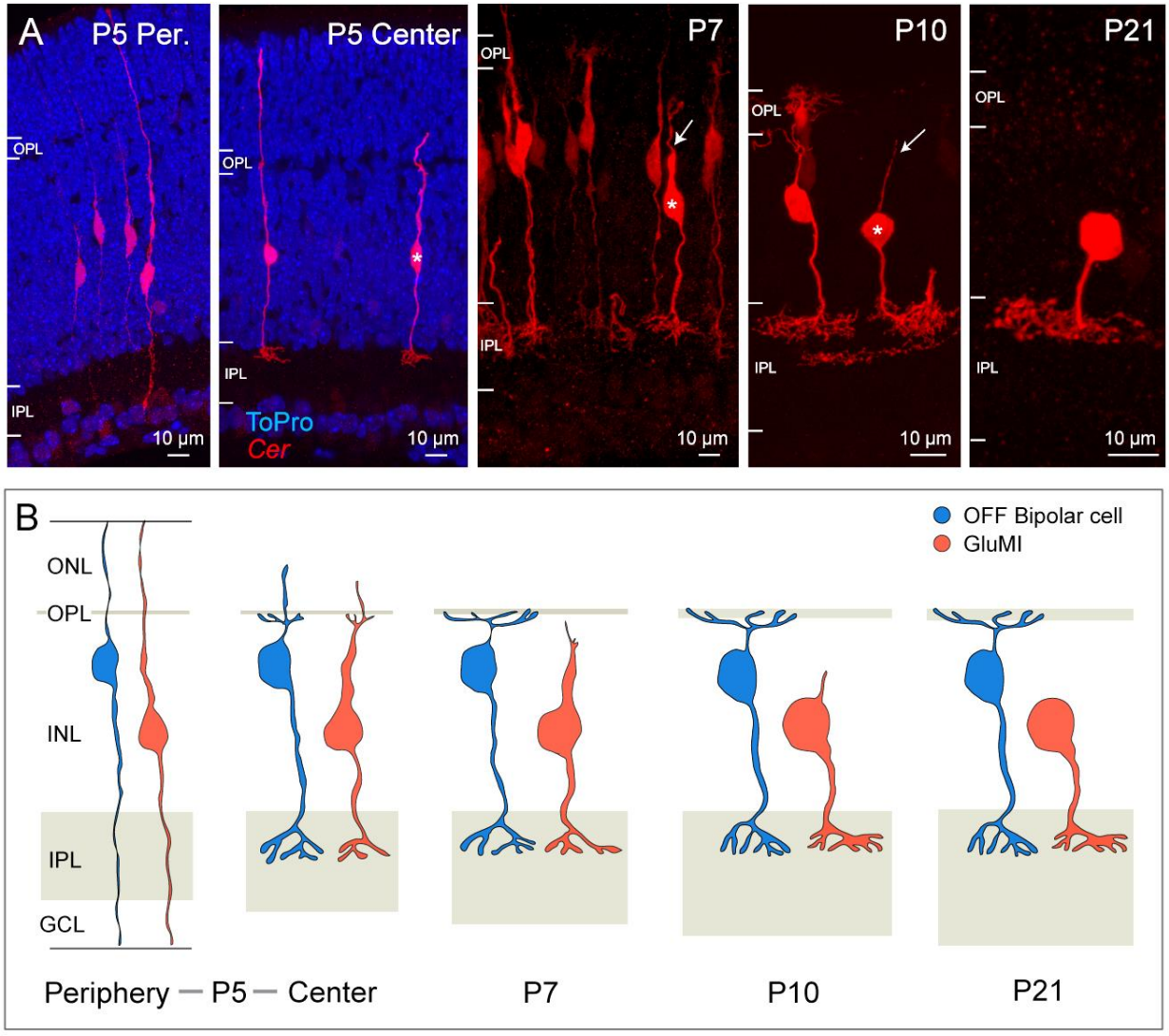
A
P5 Per.
P5 Center
P7
P10
P21
OPL
IPL
ToPro
Cer
10 µm
B
OFF Bipolar cell
GluMI
ONL
OPL
INL
IPL
GCL
Periphery — P5 — Center
P7
P10
P21

Figure S3

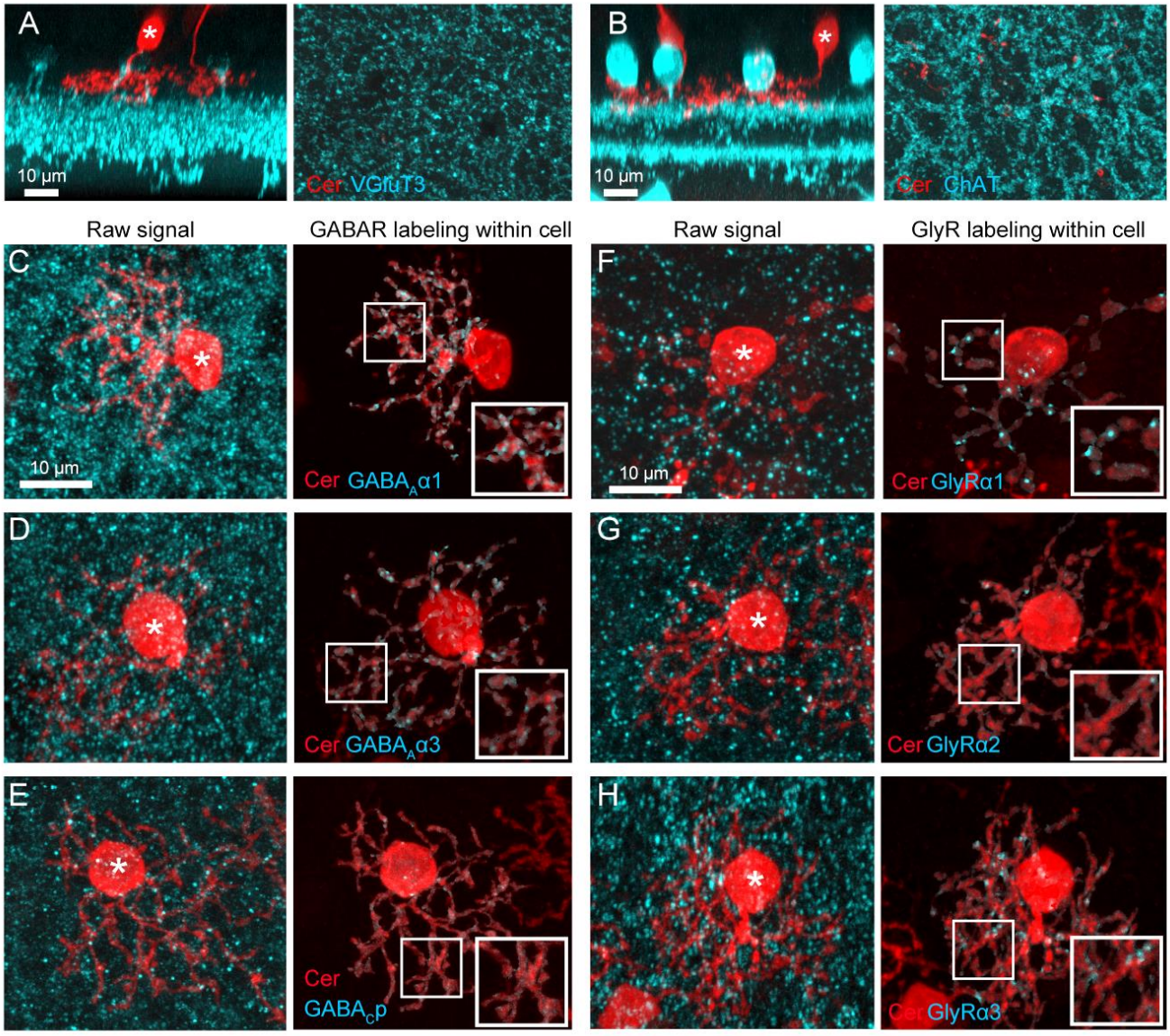
A
10 µm
Cer VGluT3
B
10 µm
Cer ChAT
Raw signal
GABAR labeling within cell
Raw signal
GlyR labeling within cell
C
10 µm
Cer GABA$_A$α1
F
10 µm
Cer GlyRα1
D
Cer GABA$_A$α3
G
Cer GlyRα2
E
Cer
GABA$_C$ρ
H
Cer GlyRα3

Figure S4

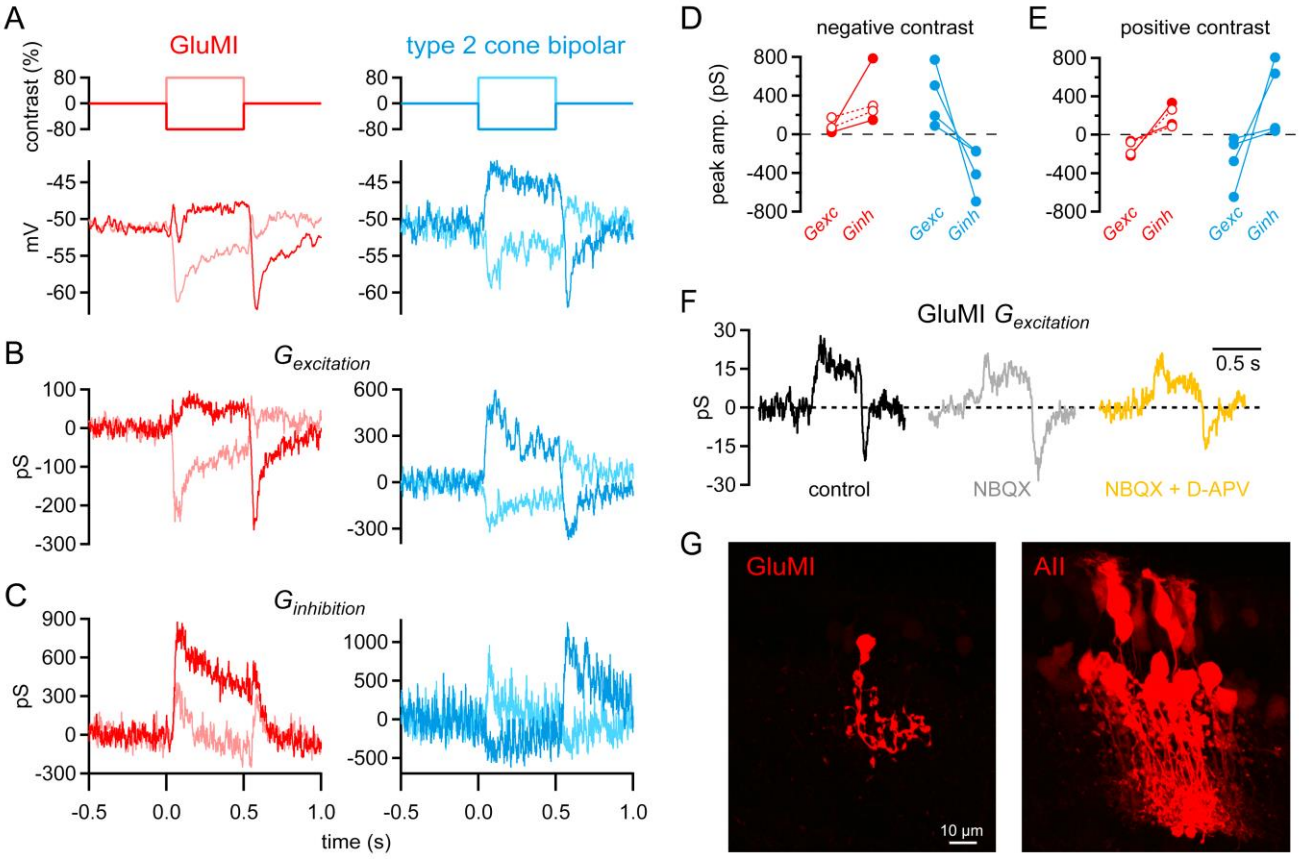
A
GluMI
type 2 cone bipolar
contrast (%)
80
0
-80
mV
-45
-50
-55
-60
B
$G_{excitation}$
pS
100
0
-100
-200
-300
600
300
0
-300
C
$G_{inhibition}$
pS
900
600
300
0
-300
1000
500
0
-500
-0.5
0.0
0.5
1.0
time (s)
D
negative contrast
peak amp. (pS)
800
400
0
-400
-800
Gexc
Ginh
E
positive contrast
F
GluMI $G_{excitation}$
pS
30
15
0
-15
-30
0.5 s
control
NBQX
NBQX + D-APV
G
GluMI
AII
10 µm

Supplemental Figure Legends

Figure S1. Related to Figure 1: GluMIs immunoreactivity for bipolar cell markers.

A, B: Immunostaining for Synaptotagmin 2, a marker of Type 2 and Type 6 cone bipolar cells. (A) Side-view of the GluMI (asterisk). (B) Single confocal plane through the arbor of the GluMI (red). Insets are 2x-magnification of the two boxed areas.
C, D: Immunostaining for the NK3 receptor (NK3R). (C) Side-view of the GluMI (asterisk). (D) Maximum intensity projection of the confocal planes encompassing the cell body of GluMI (asterisk). Inset shows NK3R staining lacking in GluMI cell body.
E, F: GluMI express Calcium Binding Protein 5 (CaBP5). (E) Side-view of the GluMI (asterisk). (F) Maximum intensity projection of the confocal planes encompassing the cell body of the GluMI (asterisk). Inset shows CaBP5 labeling within the GluMI cell body.
G: En-face view of a GluMI in the *Grm6-YFP* retina shown here for a maximum intensity projection of a confocal image stack. Immunolabeling for ribbons (anti-CtBP2) within the digitized volumetric mask of the cell (YFP signal) is shown. Inset: 2x-magnification of the boxed region.
H: Side-view of the cell in (G) showing the entire distribution of CtBP2 labeling in the region of the cell. INL, inner nuclear layer; IPL, inner plexiform layer; GCL, ganglion cell layer.

Figure S2. Related to Figure 1; Figure 2: GluMIs likely acquire their monopolar morphology upon retraction of an apical process.

A: Vertical sections of *Vsx1-cerulean* mouse retina at different developmental ages showing immature GluMI and OFF bipolar cells. Because of the central to peripheral (Per.) gradient of retinal maturation, we show here cerulean positive cells from both regions. Cell nuclei are labeled by the nuclear marker ToPro (blue) Arrows indicate apical processes that may be retracting. OPL/IPL: outer/inner plexiform layer.
B: Schematic proposing the developmental steps of an OFF cone bipolar cell and a GluMI that could lead to their differences in morphology. ONL, outer nuclear layer; INL, inner nuclear layer; GCL, ganglion cell layer.

Figure S3. Related to Figure 2: GluMIs contain GABA and glycine receptors

A-B: Immunostaining for VGluT3 and Choline Acetyl Transferase (ChAT) in *Vsx1-cerulean* (Cer) retina. Left panels represent side-view rotations of the confocal image stacks. Right panels represent maximum intensity projections of the VGluT3 and the OFF ChAT plexus in the IPL, respectively. n=5 cells from 3 mice each (VGluT3 or ChAT immunopositive) were imaged. Asterisk = GluMI.
C-E: Immunostaining for $GABA_A$ receptor subunits **α**1, **α**3 and $GABA_C$**ρ** subunits in the *Vsx1-cerulean* retina. The asterisks mark GluMIs.
F-H: Immunostaining for Glycine receptor subunits **α**1, **α**2 and **α**3 in the *Vsx1-cerulean* retina
Left panels are the maximum intensity projection images of the GluMIs (asterisks) and receptor immunostaining in the field of view.
Right panels show the receptor subunit signal only within the cell's volume masked in 3D using the Labelfield function of AMIRA (see Supplemental Experimental Procedures). Insets show higher magnification of the boxed areas. Scale bar applies to all images.

Figure S4. Related to Figure 4: Comparison of light evoked currents of GluMIs and Type 2 bipolar cells.

A: Example voltage responses of GluMI (left, red) or Type 2 cone bipolar cell (right, blue) to step increments or decrements in light intensity. Steps were delivered from a background light level of ~2000 R*/Scone/s.
B-C: Excitatory (B) and inhibitory (C) synaptic conductances to same step stimuli. Same cells as shown in (A).
D-E: Summary of negative (D) or positive (E) contrast step-evoked peak conductances in GluMIs (n=4) and type 2 cone bipolar cells (n=4). Lines connect values (circles) measured from individual cells. +/-100% contrast steps were used in recordings from two GluMIs (open circles connected by dashed lines). All other recordings used +/-80% contrast steps.
F: Example step responses (-80% contrast, 500 ms duration) from a GluMI in which excitatory currents were measured under control conditions, in the presence of NBQX (10 µM), and NBQX (10 µM) + D-APV (50 µM).

Each trace shows mean response to 10 stimulus presentations in each condition. NBQX or NBQX+D-APV did not eliminate step-evoked excitation in two additional GluMIs (n=3 cells total).

G: Example images in which a GluMI (left) or AII amacrine cell (right) was dialyzed via a patch-pipette with Neurobiotin (4% w/v in K-aspartate internal solution; retinal slice). Note that the GluMI does not show evidence for tracer-coupling whereas Neurobiotin spread to nearby amacrine and bipolar cells when the tracer was introduced into the AII amacrine cell. We did not find evidence for tracer coupling in a total of four GluMI cells dialyzed with Neurobiotin, whereas AII amacrine cells (n = 4) in the same retinal slices (four slices total) were extensively coupled to nearby neurons.

Supplemental Experimental Procedures:

Animals

Mice aged 5 to 60 days of either sex were used for experiments. All procedures were performed in accordance with the University of Washington Institutional Animal Care and Use Committee protocols.

Transgenic mice were used in which the *Vsx1* promoter drives expression of cerulean fluorescent protein [S1] or the *Grm6* promoter drives expression of YFP [S7].

Immunohistochemistry

For immunolabeling of whole mounts, retinas were isolated and four relieving cuts were made to allow the retina to lie flat on filter paper (Millipore, HABP13). Retinas were then fixed in 4% paraformaldehyde in mouse artificial cerebral spinal fluid (ACSF) (pH = 7.4) for 15 to 30 min. Mouse ACSF contains (in mM): NaCl (119), KCl (2.5), $MgCl_2$ (1.3), $CaCl_2$ (2.5), $NaHPO_4$ (1), glucose (11), HEPES (20), pH 7.4. After fixation, retinas were rinsed in 0.1 M phosphate buffered saline (PBS). For immunolabeling of retinal sections, eyecups were fixed in 4% paraformaldehyde in ACSF (pH = 7.4) for 15 to 30 min. After fixation, the eyecups were rinsed 3x10 minutes in PBS and retinas were isolated and embedded in 4% agarose in PBS, and sectioned (60 µm thick) using a microtome (Leica Microsystems).

Immunostaining was performed as follows: Wholemounted retinas were placed in 5% normal goat serum (NGS) in PBS overnight at 4^0C followed by 5 days of incubation with 5% NGS, 0.5% Triton-X100, with the primary antibody. The primary antibodies used were: rabbit polyclonal anti-GFP (1:1000; Invitrogen), mouse monoclonal anti-GAD67 (1:1000; Millipore), rabbit polyclonal anti-GAD65 (1:1000; Chemicon), mouse monoclonal anti-Syntaxin-1 (1:1000; Sigma), goat polyclonal anti-GlyT1 (1:1000; Millipore), mouse monoclonal anti-CtBP2 (1:1000; BD Biosciences), guinea-pig polyclonal anti-VGLUT1 (1:1000; Chemicon), mouse monoclonal anti-GlyR α1 (1:500; Synaptic Systems), goat polyclonal anti-GlyR α2 (1:300; Santa Cruz Biotechnology), goat polyclonal anti-GlyR α3 (1:500, Santa Cruz Biotechnology), rabbit polyclonal anti-$GABA_C$ρ (1:500; kindly provided by R.Enz), guinea-pig polyclonal anti-$GABA_A$α1 (1:5000; kindly provided by J.M. Fritschy), guinea-pig polyclonal $GABA_A$α3 (1:3000; kindly provided by J.M. Fritschy), mouse monoclonal anti-Synaptotagmin2 (1:500, ZFIN), mouse anti-CaBP5 (1:200, kindly provided by F.Haessleer), rabbit polyclonal anti-NK3R (1:500, kindly provided by A.Hirano), rabbit polyclonal anti-VGLUT3 (1:500; Synaptic Systems), goat polyclonal anti-ChAT (1:1000; Chemicon). The tissue was then washed 3x10 min in PBS and incubated overnight (flatmounts) or 2 hours (sections) at 4^0C with the secondary antibodies, conjugated to either Alexa-568 (1:1000; Invitrogen) or Dy-light 488 or Dy-light 649 (1:1000; Jackson Immunoresearch laboratories). Retinas were then washed 3x10 min in PBS and mounted onto glass slides using Vectashield (Vector).

Near-infrared branding (NIRB) and serial block face scanning electron microscopy (SBFSEM)

Vsx1:Cerulean mouse retinas were fixed in 4% glutaraldehyde in 0.1M sodium cacodylate buffer (pH7.4) for 30 min. The tissue was washed three times and flat-mounted under a coverglass in 0.1 M sodium cacodylate buffer for multiphoton imaging. An image stack was taken using a custom-built two-photon microscope with a Ti:sapphire laser (Spectra-Physics) of a region comprising fluorescently labeled cells. GluMIs were identified from the image stack based on their axonal stratification level, their soma location and the absence of dendrites. Typical Voxel dimensions of the multiphoton image stack were xy: 0.15 µm and z-step: 0.5 µm. To relocate the GluMI under electron microscopy, fiduciary marks were burned into the tissue using the near-infrared branding (NIRB) method [S2]. The laser power was typically set at 100 mW measured at the light path before the objective lens. Repeated line scans for a total duration of 10 s at a wavelength of 880 nm were performed; the laser power was increased by 20 mW at a time if burning was not apparent from the autofluorescence. A box was branded at three different tissue depths; at the cell soma, above the GluMI's arbor in the IPL, and at the RGC layer. After NIRB-ing, the retina was unmounted and fixed in 4% glutaraldehyde overnight, and then processed for SBFSEM, using a protocol provided by M. Ellisman (UCSD).

For SBFSEM, the tissue was washed 3 x 5 min (all washes) in 0.1M cacodylate buffer, pH7.4 and incubated in a solution containing 1.5% potassium ferrocyanide and 2% osmium tetroxide (OsO_4) in 0.1M cacodylate buffer (0.66% lead in 0.03M aspartic acid, pH 5.5) for 1 hour. After washing, the tissue was placed in a freshly made

thiocarbohydrazide solution (0.1g TCH in 10 ml double-distilled H_20 heated to 60^0C for 1 h) for 20 min at room temperature (RT). After another rinse, at RT, the tissue was incubated in 2% OsO_4 for 30 min at RT. The samples were rinsed again and stained en bloc in 1% uranyl acetate overnight at 4^0C, washed and stained with Walton's lead aspartate for 30 min. After a final wash, the retinal pieces were dehydrated in a graded ice-cold alcohol series, and placed in propylene oxide at RT for 10 min. Finally; NIRB-ed samples were embedded in Durcupan resin. Semi-thin sections (0.5 -1 µm thick) were cut and stained with toluidine blue, until the fiducial marks (box) in the GCL appeared. The block was then trimmed and mounted in the SBFSEM microscope (GATAN/Zeiss, 3View). Serial sections were cut at 50 - 55 nm thickness, and imaged at an x-y resolution of 5.0 - 5.5 nm. Typically, 3 x 3 tiles, each about 40 µm x 40 µm were obtained with an overlap of about 10% – the soma of the cell of interest was within the center tile. The image stacks were concatenated and aligned using TrackEM (NIH). The GluMIs were traced using the tracing tools in Track EM.

Biolistic transfection of retinal ganglion cells

After euthanasia, the eyes were removed and placed in HEPES-buffered, oxygenated mouse ACSF. Retinas were isolated from the eyecup under a dissection microscope and mounted onto nitrocellulose filter paper (Millipore HABP13). DNA coated gold particles were prepared by coating 12.5 mg of 1.6 µm gold particles (Bio-Rad) with 12 µg of PSD95-YFP plasmid. A Helios gene gun (Bio-Rad) was used to ballistically deliver plasmid-coated gold particles to the whole-mounted retinas [S3]. Retinas were then transferred to an oxygenated and humidified chamber and maintained for 29 hours at 32°C, allowing fluorescent protein to be expressed sufficiently for subsequent imaging.

Image acquisition and analysis

Image stacks were acquired using an FV1000 laser scanning confocal microscope (Olympus). Fixed tissue was imaged using a 1.35 NA 60x oil immersion objective at a voxel size of 0.069, 0.069, 0.3 µm or 0.051, 0.051, 0.3 µm (x, y, z) for images used for masking and quantification of individual GluMI. Voxel size of 0.103, 0.103, 0.3 µm (x, y, z) was used for imaging the ganglion cells. Each optical plane was averaged three to four times (Kalman filter). Raw image stacks were processed using ImageJ [S4] and Amira (FEI). For receptor masking within GluMIs, the cerulean signal of GluMI neurites was masked in three dimensions using the ''label field'' function of Amira. Subsequently, this volumetric mask was multiplied with the receptor or CtBP2-labeled channel to isolate labeling within the GluMI neurites. Measurements of GluMI soma and arbor size were obtained by quantification of the area for the convex hull containing the soma or the arbor, then reported as diameter of a circle with equivalent area.

Physiological recordings

Whole-cell current- or voltage-clamp recordings were obtained in 200 um-thick retinal slices (GluMIs, Type 2 bipolar cells) or flat-mount retina (A_{OFF-S} RGCs) from 3-5 week-old *Vsx1-cerulean* (GluMIs) or wild-type (Type 2 bipolar cells, A_{OFF-S} RGCs) mice. In all cases, we restricted recordings to ventral retina. Mice were dark-adapted overnight prior to use and all tissue preparation was performed under infrared (>950 nm) illumination. Slices and flat-mounts were prepared as described previously [S5,S6].

To target GluMIs, cerulean-expressing cells in *Vsx1*-cerulean tissue were identified using two-photon laser scanning microscopy (880 nm). Putative GluMIs were distinguished from bipolar cells by the closer proximity of their somata to the inner plexiform layer. We minimized light exposure from the two-photon laser by restricting scan regions (85 µm x 85 µm) to the inner retina, away from photoreceptors, and limiting scanning time to <1 min per scan region. Post-objective laser power was always kept below 2 mW. After identifying potential GluMIs, cells were patched using differential interference contrast microscopy and infrared illumination (> 950nm). Using these parameters, light responses in slices are not affected at the background light levels used here (S. Kuo and F. Rieke, unpublished).

During recordings, retinal tissue was constantly perfused at ~8mL/min with oxygenated (95% O_2, 5% CO_2), bicarbonate-buffered Ames' solution (Sigma) maintained at 30-34°C. Patch electrodes for recordings from GluMIs or Type 2 bipolar cells (8-10 MΩ) were filled with an internal solution containing (in mM): 123 K-aspartate, 10 KCl, 10 HEPES, 1 $MgCl_2$, 1 $CaCl_2$, 2 EGTA, 4 Mg-ATP, 0.5 Tris-GTP, and 0.1 Alexa Fluor 594 hydrazide (~280 mOsm; adjusted to pH 7.2, using KOH). Voltages are corrected for a measured liquid junction potential of -10.8 mV. Series resistance was not compensated in voltage-clamp recordings from GluMIs or bipolar cells. For voltage-clamp recordings, cells were clamped at -70 mV or 0 mV, near the calculated reversal

potentials for Cl^- or cation-mediated conductances, respectively. No bias current injection was applied during current-clamp recordings. Following every recording, cells were visualized using two-photon excitation of Alexa Fluor 594 to confirm the recorded cell had GluMI (n=5/5 recordings) or Type 2 bipolar-like (n=6/6 recordings) morphology. Type 1 and Type 2 bipolar cells can be difficult to distinguish based on morphology alone. We therefore additionally included Lucifer Yellow CH, Li^+ in the pipette solution (0.33 mM) when attempting recordings from Type 2 bipolar cells. After recordings, retinal slices were fixed in 4 % paraformaldehyde dissolved in mouse artificial cerebrospinal fluid (mACSF) for 30 min at room temperature, and washed in phosphate-buffered saline (PBS) three times. mACSF contains (in mM) 119 NaCl, 2.5 KCl, 2.5 $CaCl_2$, 1.3 $MgCl_2$, 1 NaH_2PO_4, 11 glucose and 20 HEPES. Fixed slices were then incubated overnight at 4°C with anti-Lucifer Yellow antibody (1:1000, rabbit, Invitrogen) and anti-Synaptotagmin-2 antibody (znp-1, mouse, 1:1000, Zebrafish International Research Center) diluted in PBS that contained 5% normal donkey serum and 0.5% Triton-X 100. Subsequently, slices were incubated for 2 hours at room temperature with secondary antibodies conjugated with Alexa Fluor 488 (1:1000, Invitrogen) or DyLight Fluor 649 (1:1000, Jackson ImmunoResearch). We successfully confirmed recorded cells with putative Type 2 bipolar morphology also expressed synaptotagmin2 in 4 out of 6 recordings. We identified $A_{OFF\text{-}S}$ RGCs for recordings in flat mount retina by using cell-attached recordings of spike responses to ~10 R*/rod/s steps of light from darkness [S7]. For $A_{OFF\text{-}S}$ RGC recordings, patch electrodes (~2-3 MΩ) were filled with an internal solution containing (in mM): 105 Cs-methanesulfonate, 10 Tetraethylammonium-Cl, 20 HEPES, 10 EGTA, 2 QX-314, 5 Mg-ATP, 0.5 Tris-GTP; ~280 mOsm; pH adjusted to 7.3 using CsOH. For these recordings, series resistance (<10 MΩ) was compensated by 70% using the amplifier circuitry. The strong ON pathway-derived (cross-over) inhibition in $A_{OFF\text{-}S}$ RGCs [S7] provided a convenient way to empirically determine the holding potential at which to voltage-clamp cells to isolate excitatory conductances; we measured step responses and varied the holding potential over a small range around ~-70mV and chose the potential at which cross-over inhibition was nulled.

Light stimuli were focused on the slice through the microscope condenser. A short wavelength light-emitting diode (peak spectral output at 395 nm; Hosfelt) was used to present spatially uniform light stimuli over a 540 µm diameter circular region centered on the recorded cell. Stimulus contrast was defined as: (S – B) / B, where S is stimulus intensity and B is background light intensity. Light responses were measured upon a background light intensity of ~2000 photoisomerizations (R*) per short wavelength opsin-expressing cone (Scone) per second, which was equivalent to ~3000R*/rod/s (calculated assuming a collecting area of 0.2 μm^2 and 0.5 μm^2 for cones [S8] and rods [S9], respectively).

Physiological data analysis

Linear-nonlinear models of GluMI and Type 2 bipolar cell light responses were derived from responses to randomly fluctuating light stimuli (Gaussian distribution of light intensities with standard deviation = 50% of mean intensity; 0-60Hz bandwidth) as previously described [S10,S11]. Briefly, the linear filter was calculated by computing the cross-correlation of the light stimulus with the measured response and dividing the result by the power spectrum of the stimulus. The static nonlinearity was then constructed from a point-by-point comparison of the predicted filter output (convolution of stimulus with linear filter) with the measured response and binning the result along the x-axis (200 ~equal sized bins). To generate LN model predictions, nonlinearities were fit with a cumulative Gaussian function: $f(x) = \alpha C(\beta x + \gamma) + \delta$, where $C()$ is the cumulative normal density and $\alpha, \beta, \gamma,$ and δ are parameters selected to provide the best least-squares fit to the data [27].

For each filter, we calculated a biphasic index = |T| / |P|, where P = maximum amplitude of first (primary) filter lobe and T = maximum amplitude of the second filter lobe. Nonlinearity shape was quantified using a rectification index = (a + b) / (a – b), where a = maximum depolarization (of nonlinearity; see Fig. 4G) in response to negative contrast stimuli, relative to the resting membrane potential, and b=largest hyperpolarization to increments relative to resting potential. Nearly identical rectification indices were calculated when area of the nonlinearity curve above and below baseline was used instead of maximal depolarization/hyperpolarization.

Excitatory (G_{exc}) and inhibitory (G_{inh}) synaptic conductances in GluMIs or type 2 bipolar cells were calculated from step-evoked currents (I) measured near the inhibitory ($E_{inh} = -59$ mV) or excitatory ($E_{exc} = 0$ mV) reversal potential, respectively:

$$G_{exc} = \frac{I}{V_{hold} - E_{exc}};$$

$$G_{inh} = \frac{I}{V_{hold} - E_{inh}}$$

where V_{hold} is the holding potential at which the cell was voltage-clamped.

We used the same Gaussian noise stimulus as for GluMI and Type 2 bipolar recordings to assess responses in $A_{OFF\text{-}S}$ RGCs. Because we wished to examine whether light-driven excitatory inputs to $A_{OFF\text{-}S}$ RGCs had multiple components, we used current-weighted covariance, analogous to traditional spike-triggered covariance analysis [S12,S13], to analyze $A_{OFF\text{-}S}$ RGCs responses. We calculated the current-weighted stimulus covariance matrix (C):

$$C = \frac{1}{N}\sum_{n=1}^{N}[\,(\vec{s}(t_n)\ \times\ |r(t_n)|) - A][(\vec{s}(t_n)\ \times\ |r(t_n)|) - A]^T$$

where N is the total number of time points in the response (5 ms resolution), $\vec{s}(t_n)$ is the stimulus vector corresponding to the 300 ms window preceding the time point, t_n, $|r(t_n)|$ is the absolute value of the excitatory current measured at time, t_n, $[...]^T$ denotes the transpose of the vector in […], and A is the response-weighted average:

$$A = \frac{1}{N}\sum_{n=1}^{N}[\,(\vec{s}(t_n)\ \times\ |r(t_n)|)$$

Similarly, we calculated the covariance matrix of the prior distribution of stimuli (C^{prior}):

$$C^{prior} = \frac{1}{N}\sum_{n=1}^{N}[\,(\vec{s}(t_n)\ \times\ |\bar{r}(t)|)][(\vec{s}(t_n)\ \times\ |\bar{r}(t)|)]^T$$

where $\bar{r}(t)$ is the mean value of the response.

To identify the stimuli for which the variance was different from the prior distribution of stimuli, we then subtracted the covariance matrix of the prior from the current-weighted stimulus covariance matrix to get a matrix of covariance differences, C^{diff}:

$$C^{diff} = C - C^{prior} \qquad (4)$$

Finally, we diagonalized the matrix C^{diff} to find its eigenmodes and corresponding eigenvalues (see Figure 4J) and selected those eigenmodes ('features') for which the eigenvalue was clearly larger or less than zero. Nonlinearities for each of these features were calculated separately as described above for the LN models. We confirmed these one-dimensional nonlinearities were an accurate representation of the two-dimensional nonlinearity constructed from the different filter predictions and measured response (i.e. the two-dimensional nonlinearity was separable).

Neurobiotin cell fills

Retinal slices from dark-adapted *Vsx1-cerulean* mice were prepared as for physiological recordings (see above) and whole-cell patch-clamp recordings were established from GluMIs or AII amacrine cells using pipettes filled with K-aspartate internal solution (see above) and 4% w/v Neurobiotin tracer (Vector Laboratories) and 0.1

mM Alexa Fluor 594. In these experiments, identical procedures (e.g. dark conditions) were used as for physiological recordings, but we did not collect physiological data from the cells because inclusing of Neurobiotin in the pipette solution altered the Cl^- reversal potential. After allowing the pipette solution to dialyze the recorded cell for 10 minutes, cells were visualized using two-photon excitation of Alexa Fluor 594 to confirm identity of the patched cell, and then the pipette was carefully removed. In each slice, we patched at least one GluMI and one AII amacrine cell in the same slice before fixing the tissue in 4% paraformaldehyde in PBS for 30 minutes at room temperature then washing three times in PBS. Thereafter the neurobiotin signal was amplified by overnight incubation at 4^0C in blocking solution (PBS with 5% NGS and 0.5% Triton-X100) containing streptavidin conjugated to Alexa Fluor 568 (1:200, Invitrogen). Images were acquired on an Olympus FV1000 laser scanning confocal microscope, using a 1.35NA 60X Objective. Raw image stacks were processed using MetaMorph (Universal Imaging) and Amira (Mercury Computer Systems) software. We did not find evidence for strong tracer coupling in a total of four GluMIs in four slices, whereas AII amacrine cells filled in the same slices were extensively coupled to nearby amacrine and bipolar cells (see examples in Figure S4G).

Supplemental References

S1. Hoon, M., Sinha, R., Okawa, H., Suzuki, S.C., Hirano, A.A., Brecha, N., Rieke, F., and Wong, R.O.L. (2015). Neurotransmission plays contrasting roles in the maturation of inhibitory synapses on axons and dendrites of retinal bipolar cells. Proc. Natl. Acad. Sci. U.S.A. 112, 12840–12845.

S2. Bishop, D., Nikić, I., Brinkoetter, M., Knecht, S., Potz, S., Kerschensteiner, M., and Misgeld, T. (2011). Near-infrared branding efficiently correlates light and electron microscopy. Nat. Methods. 8, 568–570.

S3. Okawa, H., Santina, Della, L., Schwartz, G.W., Rieke, F., and Wong, R.O.L. (2014). Interplay of cell-autonomous and nonautonomous mechanisms tailors synaptic connectivity of converging axons in vivo. Neuron. 82, 125–137.

S4. Schneider, C.A., Rasband, W.S., and Eliceiri, K.W. (2012). NIH Image to ImageJ: 25 years of image analysis. Nat. Methods. 9, 671–675.

S5. Armstrong-Gold, C.E., and Rieke, F. (2003). Bandpass filtering at the rod to second-order cell synapse in salamander (Ambystoma tigrinum) retina. J. Neurosci. 23, 3796–3806.

S6. Grimes, W.N., Schwartz, G.W., and Rieke, F. (2014). The synaptic and circuit mechanisms underlying a change in spatial encoding in the retina. Neuron. 82, 460–473.

S7. Murphy, G.J., and Rieke, F. (2006). Network variability limits stimulus-evoked spike timing precision in retinal ganglion cells. Neuron. 52, 511–524.

S8. Nikonov, S.S., Kholodenko, R., Lem, J., and Pugh, E.N. (2006). Physiological features of the S- and M-cone photoreceptors of wild-type mice from single-cell recordings. J. Gen. Physiol. 127, 359–374.

S9. Field, G.D., and Rieke, F. (2002). Mechanisms regulating variability of the single photon responses of mammalian rod photoreceptors. Neuron. 35, 733–747.

S10. Kim, K.J., and Rieke, F. (2001). Temporal contrast adaptation in the input and output signals of salamander retinal ganglion cells. J. Neurosci. 21, 287–299.

S11. Rieke, F. (2001). Temporal contrast adaptation in salamander bipolar cells. J. Neurosci. 21, 9445–9454.

S12. Fairhall, A.L., Burlingame, C.A., Narasimhan, R., Harris, R.A., Puchalla, J.L., and Berry, M.J. (2006). Selectivity for multiple stimulus features in retinal ganglion cells. J. Neurophysiol. 96, 2724–2738.

S13. Schwartz, O., Pillow, J.W., Rust, N.C., and Simoncelli, E.P. (2006). Spike-triggered neural characterization. J Vis. 6, 484–507.